THE JOURNAL OF PHYSICAL CHEMISTRY C

Article

Cite This: J. Phys. Chem. C 2019, 123, 28997−29007

pubs.acs.org/JPCC

Amine-Phosphate Specific Interactions within Nanochannels: Binding Behavior and Nanoconfinement Effects

Gregorio Laucirica,[†] Gonzalo Pérez-Mitta,[†,∥] M. Eugenia Toimil-Molares,[‡] Christina Trautmann,[‡,§] Waldemar A. Marmisollé,*[,†] and Omar Azzaroni*[,†]

[†]Instituto de Investigaciones Fisicoquímicas Teóricas y Aplicadas (INIFTA), Departamento de Química, Facultad de Ciencias Exactas, Universidad Nacional de La Plata (UNLP) - CONICET, Diagonal 113 y 64, 1900 La Plata, Argentina

[‡]GSI Helmholtzzentrum für Schwerionenforschung, 64291 Darmstadt, Germany

[§]Technische Universität Darmstadt, 64287 Darmstadt, Germany

Supporting Information

ABSTRACT: In the last years, the ionic conductance behavior of solid-state nanochannels (SSN) has been extensively studied with both basic and applied purposes. In particular, the interactions between confined groups and dissolved species have been widely used for the design of biosensors and smart devices. Being the species confined to the small volume of the SSN, the ionic equilibrium usually differs from that in the solution bulk and nanoconfinement effects appear. In this work, we study the binding equilibrium between surface-confined amine groups and phosphate anions taking place within SSN by measuring the changes in the iontronic transmembrane current response of single nanochannels at different phosphate concentrations. Phosphate binding is higher compared with other divalent anions and takes place even in electrostatically hindered conditions, which reinforces the idea of chemical specificity of the amine-phosphate interaction. The sensitivity of the iontronic response of asymmetric SSN to changes in the surface charge allowed the interpretation of the experimental results in terms of a simple binding model, which reveals that the nanoconfinement effects are responsible for a one order of magnitude increase in the effective constants for the anion binding to the surface amine groups in the nanochannel walls. Furthermore, polyphosphates show a more pronounced binding tendency toward amine moieties, which allows the detection and quantification of ATP in the micromolar range from the analysis of the iontronic response.

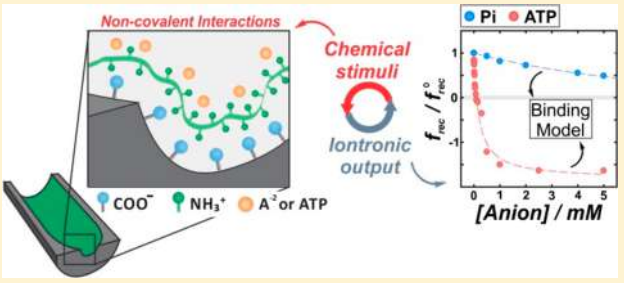

1. INTRODUCTION

Nature has been always used as a source of inspiration for the development of devices for diverse applications.[1−4] An example is the design of fully abiotic nanochannels commonly called solid-state nanochannels (SSN),[5−7] inspired by the ion channels present in cells.[8] Ion channels are proteins embedded in the plasma membrane that allow the flux of ions from external medium to internal medium and vice versa, playing a fundamental role in several processes such as the excitation−contraction coupling in muscles and nerve impulse transmission.[8] Biological ion channels also present several interesting properties facing the development of abiotic smart platforms, such as rectification of ionic current and responsiveness to physical and chemical stimuli. In this sense, the activity of several ion channels is regulated by environmental conditions. In some channels, the presence of specific moieties can trigger its opening or closing (gating). For example, the ATP sensitive potassium ion channel (K_{ATP}) is gated shut when the cytoplasmic ATP exceeds the concentration of ∼100 μM.[9−11] The gating dynamics of K_{ATP} by cytoplasmic ATP plays a predominant role in the secretion of insulin from pancreatic β-cells.[12]

Regarding SSN, previous works have reported the development of devices that rectify the ionic current through the design of charged channels with asymmetric geometries.[13−16] Rectification implies that the ion flux is favored at one polarity of voltage. This phenomenon is produced by the rupture in the symmetry of the channel's inner surface axial electric potential distribution and the interactions between the ions and the charged surface.[17,18] In addition, it has been found that the degree (efficiency) of rectification is related to the magnitude of surface charge.[5,15,19,20] As a consequence, using different modification strategies to control the surface charge of SSN, it is possible to obtain *iontronic* devices for a variety of application such as biosensing, energy conversion, and filtration.[21−29]

Received: August 20, 2019
Revised: October 7, 2019
Published: October 23, 2019

DOI: 10.1021/acs.jpcc.9b07977
J. Phys. Chem. C 2019, 123, 28997−29007

One of the great aims of SSN research is the development of devices with precise control of ionic transport by different stimuli.[6,30−41] In this regard, interactions between confined groups and dissolved ions have been extensively used for the design of biosensors and smart devices.[24,42−48] On the other hand, the sensitivity of these systems to changes in the surface charge makes these devices good candidates as platforms for physicochemical studies too.[29] In this sense, an important issue connected to SSN is that the presence of a high net surface charge added to a high surface-to-volume relation and surface curvature generated complex phenomena. As an example, several authors have reported a shift in the acid−base equilibrium constants of polyelectrolytes confined within nanochannels.[49,50]

In this regard, polyamine−phosphate interactions have been also employed for the construction of different abiotic nanoarchitectures based on supramolecular assemblies.[51−57] The importance of this interaction resides in that both groups are present in multiple chemical and biological systems. In particular, the binding of amines and phosphate anions plays a key role in the self-assembly of multiple biological supramolecular structures, such as the nuclear aggregates of polyamines, which are present in many replicating cells.[58,59] A crucial aspect of the interaction of phosphate anions with polyamine-modified surfaces is the charge reversion phenomenon: as a consequence of the anion binding, positively charged amino-functionalized surfaces acquire a negative net surface charge.[60−62] This charge reversion yields even functional consequences with in vivo implications.[63,64] In this sense, we have recently studied the binding of phosphate anions to amine groups employing silica microparticles capped with poly(allylamine hydrochloride) (PAH).[63,65,66] There, we developed a binding model to quantitatively interpret the charge reversion and the dependence of the zeta potential on the phosphate concentration at several pH values. We showed that phosphate anions promote the protonation of amino groups and, conversely, charged amines induce further proton dissociation of phosphates, yielding a complex dependence of the surface effective charge on pH. Even more, those results indicated that phosphate−amine interaction is specific and the modulation of surface charge of the amino-functionalized surface by simple phosphate anions occurs in the physiological phosphate concentration range, emphasizing its biochemical relevance.[63] We have also proved that the same kind of binding takes place when amino-functionalized nanochannels are exposed to phosphates, producing changes in the iontronic response.[67]

In the present work, we extended the study of the phosphate−polyamine interactions within nanochannels, focusing on the nanoconfinement effects by comparison with results on microparticles at various pH values. For this purpose, we carried out an extensive study on the polyamine−phosphate interactions by functionalization of single nanochannels with PAH and by studying the transmembrane current behavior as a function of the bulk concentration of phosphates. The sensitivity of the iontronic response of asymmetric SSN to changes in the surface charge allowed the interpretation of the experimental results in terms of a binding model. Particularly, the rectification factor of the asymmetric iontronic response correlates with the surface charge density,[67] which allows one to obtain physicochemical information on the surface binding phenomena. Our results give arguments in favor of the hypothesis of a specific interaction between amine groups and phosphates beyond a simple electrostatic interaction, as binding takes place even in electrostatically hindered conditions, i.e., when the net surface charge is the same of that of the binding species. Additionally, control experiments employing other divalent anions allowed us to verify the specificity of the phosphate binding within nanochannels. The nanoconfinement effects are responsible for a one order of magnitude increase in the effective binding constant of divalent anions to the surface amine groups in the nanopore walls. Finally, based on the high affinity of phosphate species toward amine-functionalized surfaces, we studied the binding behavior of polyphosphate species. In this sense, the iontronic response of PAH-functionalized single nanochannels is also shown to be sensitive toward ATP in the micromolar concentration range.

2. EXPERIMENTAL SECTION

2.1. Chemicals. Poly(allylamine) hydrochloride (PAH, $M_W \sim 17$ kDa), KCl, and HEPES were purchased from Sigma-Aldrich; NaOH and HCl were from Anedra; oxalic acid and KH_2PO_4 were from Carlo Erba; and K_2SO_4 was from Merck. ATP was purchased from Calzyme, and the surfactant Dowfax 2A1 was from Dow Chemical. All chemicals were used as received without further purification. Milli-Q water (18.2 mΩ cm, Millipore) was employed.

2.2. Chemical Etching. Bullet-like nanochannels were formed by *ion-track-etching*[26] of 12 μm thick polyethylene terephthalate (PET) membranes (Hostaphan RN 12, Hoechst). The *ion tracks* were produced by irradiating PET membranes with single ions at the linear accelerator UNILAC (GSI, Helmholtz Centre for Heavy Ion Research, Darmstadt, Germany) using Au ions of 2 GeV kinetic energy. The irradiated membranes were asymmetrically etched with a surfactant-assisted chemical procedure for 6 min at 60 °C.[27] One membrane face (base side) was exposed to 6 M NaOH, whereas the other side (tip side) was exposed to 6 M NaOH with 0.05% v/v Dowfax 2A1 added as surfactant. After etching, the membranes were thoroughly rinsed and kept in Milli-Q water overnight. Under this etching condition, channels with a base diameter of 500 nm and a tip diameter around ∼30 nm are formed (Figure S1).[22,43,44]

2.3. Polyamine Functionalization. Etched membranes were soaked in 1 mg mL^{-1} PAH, 50 mM KCl, pH 7 solution for 4 h to ensure the complete electrostatically driven adsorption. Then, membranes were washed with Milli-Q water.

2.4. *I*−*V* Measurements. Conductimetric measurements were carried out with a potentiostat (Gamry Reference 600) using a four-electrode setup: working electrode (Pt), reference 1 (Ag/AgCl), reference 2 (Ag/AgCl), and counter electrode (Pt). The working electrode was placed facing the tip side. To obtain the conductometric *I*−*V* curves, cyclic voltammetry was performed between −1 and +1 V at a rate of 100 mV s^{-1}. All solutions were prepared in 1 mM HEPES 0.1 M KCl as supporting electrolyte.

2.5. Rectification Factors. The degree of asymmetry of the *I*−*V* curves (diodelike behavior) was accounted by the rectification factor (f_{rec}), defined as follows[43]

$$f_{rec} = -\frac{|I(+1\ V)|}{|I(-1\ V)|} \quad \text{if} \quad |I(+1\ V)| > |I(-1\ V)| \quad (\text{negative } f_{rec} \text{ values}) \tag{1}$$

DOI: 10.1021/acs.jpcc.9b07977
J. Phys. Chem. C 2019, 123, 28997−29007

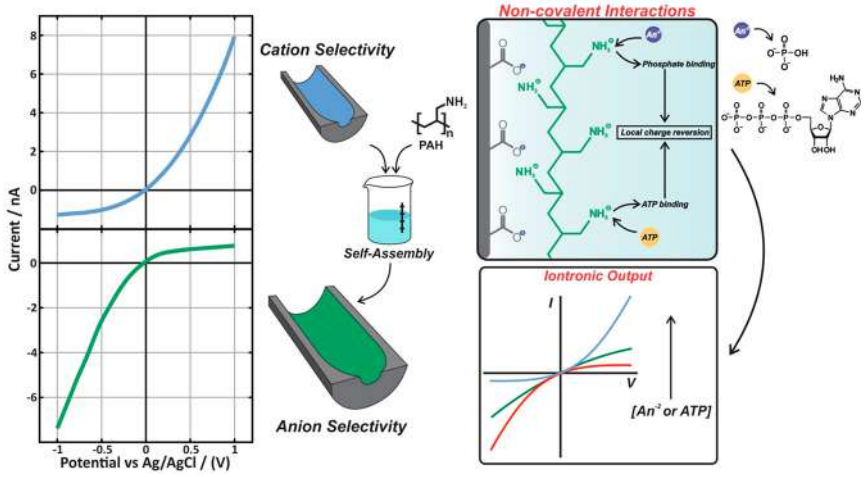

Figure 1. Scheme of the functionalization steps for a bullet-like single nanochannel and the binding and acid−base equilibriums considered in the model (right). Typical $I-V$ curves before (blue) and after (green) the functionalization with PAH (left).

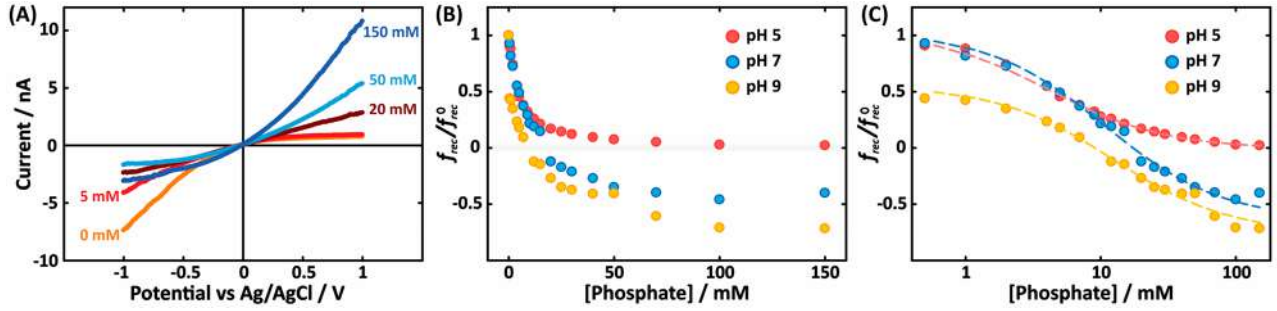

Figure 2. (A) $I-V$ curves of the modified single nanochannel for different concentrations of phosphate. All measurements were carried out in 0.1 M KCl at pH 7. (B) Experimental dependence of the relative rectification factor on the concentrations of phosphate at different pH values: 5, 7, and 9. (C) Semilog plot showing the experimental relative rectification factors (circles) and the fittings (dashed lines) to the binding model.

$$f_{rec} = \frac{|I(-1\ V)|}{|I(+1\ V)|} \quad \text{if} \quad |I(+1\ V)| \leq |I(-1\ V)|$$

$$(\text{positive } f_{rec} \text{ values}) \qquad (2)$$

where currents correspond to the extreme potential values and the current in the numerator is chosen as that of the high conductance branch, so that $|f_{rec}| \geq 1$. Furthermore, using this definition, positive values are obtained when the current branch for negative potentials is higher than that for positive potentials; which means positive surface charge density in the nanochannel walls. Inversely, negative f_{rec} values would indicate negative surface charges.[68]

3. RESULTS AND DISCUSSION

3.1. Effect of Phosphate Anions. The effect of phosphate anions (Pi) on the transport characteristics of the PAH-modified nanochannels was studied by recording current−voltage characteristics ($I-V$ curves) for increasing Pi concentrations (Figure 1).

Figure 1 shows the $I-V$ curves for a characteristic diode-like nanochannel before and after the functionalization by PAH adsorption. After etching, the nanochannel shows a cation-driven rectification due to the negative surface charge caused by deprotonation of the −COOH residues on the surface of the etched PET and the disruption of symmetry of the electric potential generated due to the bullet-shaped geometry of the pore mouth.[13,69,70] After PAH adsorption, the iontronic response gets inverted: the diode-like behavior now is ascribed to the positive surface charge, causing the anion-driven rectified transmembrane current.[68] Control experiments on nonfunctionalized track-etched nanochannels indicate that this effect is because of the presence of PAH on the nanochannels wall (Figure S2).[68]

In the presence of phosphate anions, this iontronic response changes again, even when recorded at the same pH. Figure 2A shows the $I-V$ curves in the presence of different phosphate concentrations in 0.1 M KCl at pH = 7. The corresponding $I-V$ curves at pH = 5 and pH = 9 are presented in the Supporting Information (Figure S3).

Changes in the ionic current when adding 5 mM phosphate to the electrolyte solution can be assigned to a lowering of the nanochannel positive surface charge by anion binding.[43,63] By adding more phosphate to the solution, the current keeps decreasing; and at about 20 mM Pi, a symmetric nearly linear $I-V$ curve is obtained. This ohmic behavior indicates that the surface charge density is practically null. Upon adding more phosphate to the electrolyte solution, a new asymmetric response is obtained, indicating now the preponderance of negative charges on the nanochannel walls. Thus, the ionic transport turns into cation-selective. In this new iontronic regime, the asymmetry becomes slightly more pronounced as the phosphate concentration increases.

The phosphate-induced changes in the iontronic behavior can be better analyzed in terms of the rectification factor (f_{rec}) as a function of the phosphate concentration (Figures 2B and

DOI: 10.1021/acs.jpcc.9b07977
J. Phys. Chem. C 2019, 123, 28997−29007

Table 1. Results of the Fitting of the Anion Concentration Dependence of the Rectification Factor to the Binding Model Equation at Different pH Values[a]

pH	anion	C/mM^{-1}	K_B/mM^{-1}	$[An]_0$ /mM	R (%)	$K_{B,MP}$/mM^{-1}[b]
5	phosphate	0.006 ± 0.001	0.21 ± 0.01	167	4%	0.025
7	phosphate	0.058 ± 0.003	0.105 ± 0.009	17	57%	0.082
9	phosphate	0.111 ± 0.003	0.11 ± 0.02	9	77%	0.050
7	sulfate	−0.011 ± 0.001	0.11 ± 0.01			0.013
7	oxalate	−0.002 ± 0.002	0.12 ± 0.01			0.015
7	ATP	10 ± 1	4.8 ± 0.8	0.1	209%	

[a]Standard errors of the fittings are also included. [b]These values correspond to the fitting of data from PAH-functionalized silica microparticles.[63]

S3C). Initially, f_{rec} is positive due to the positive surface charge, then it decreases owing to the decrease in the positive surface charge by phosphate adsorption, and finally it becomes negative due to the surface charge reversion, reaching an asymptotic value for high phosphate concentrations. In Figure 2B, these results are presented as relative values f_{rec}/f_{rec}^0 (where f_{rec}^0 corresponds to the solution without phosphate added in each case), to eliminate differences coming from small diameter changes when comparing different nanochannels, as previously reported for PAH-functionalized single nanochannels.[44] Absolute values recorded at different pH values are presented in Figure S3.

The results obtained when measuring the phosphate influence at other pH values are similar (Figure 2B). In the case of pH 5, however, the asymptotic limit for high phosphate concentrations lays in the isoelectric region (near null surface charge), indicating that no charge reversion is achieved in this more acidic pH condition.

On the other hand, at pH 9 the rectification factors for high phosphate concentrations are even more negative than those obtained at pH 7, which clearly indicates that more negative surface charge values are attained (Figure S3). It is important to note that the surface charge density slightly decreases even in the negative regime, indicating that the association of phosphate anions takes place even when it is electrostatically hindered.

Thus, surface charge neutralization seems not to be the only driving force for phosphate binding. On the other hand, the limit obtained for high phosphate concentrations depends on the solution pH, which indicates that the acid−base dissociation equilibrium of surface groups, both amino and bound phosphate anions, should be considered.

Considering the binding of anionic species to charged amine surface groups and the acid−base dissociation equilibriums, we developed a binding model to account for the dependence of the rectification factor on the concentration of binding species. According to this model, the rectification factors present the following general dependence on the anion bulk concentration [An] as

$$f_{rec} = f_{rec}^0\left(\frac{1 - C[An]}{1 + B[An]}\right) \quad (3)$$

where B and C are constants related to the binding and acid−base equilibrium constants as explained in the Appendix and f_{rec}^0 is the rectification factor in the absence of binding anions. In the case of phosphate anions, in the pH range from 4 to 9, the relevant species are the monovalent and divalent ones. In this case, [An] corresponds to the total phosphate concentration, [Pi]. From eq 3, it is possible to define the anion concentration for inducing zero net surface charge as $[An]_0 = C^{-1}$ (eq A.17) and the charge reversion degree, $R(\%)$, as $R(\%) = 100(C/B)$ (see eq A.18).

Figure 2C also presents the predicted values (dashed lines) from the fitting of the experimental points to the model equation in the case of the phosphate binding at several pH values. The good agreement of the fittings with the experimental data suggests that the binding model is adequate for the quantitative description of the rectification behavior. The binding model parameters determined by nonlinear fitting for the simple phosphate anions are presented in Table 1.

A similar analysis has been previously performed for the binding of phosphate species to PAH-functionalized silica microparticles by means of zeta potential determination. In that case, differences in the pH dependence of the effective binding constants were interpreted in terms of the binding of monovalent and divalent phosphate anions. The divalent anion was shown to bind with a constant 5 times higher than that for the monovalent anion. This differential binding leads to a shift in the monovalent-divalent equilibrium of surface-bound phosphates to the formation of divalent species.

In the present case, however, the comparison between the binding equilibrium in nanochannels and in microparticles reveals the effect of nanoconfinement on the interplay between phosphate binding and acid−base equilibriums. First, the effective phosphate binding constants are higher in the case of the nanochannels (Figure 3). Nanoconfinement essentially leads to the depletion of co-ions and the enrichment of counterions inside the nanochannels as compared with bulk concentrations.[20]

Although the binding affinity in nanochannels is higher in the whole pH range, the increment of the binding constant is markedly higher at pH 5 (Figure 3). At this pH, the surface charge density of the nanochannel wall remains positive even for high phosphate concentrations. This fact triggers the accumulation of anions in the nanoconfined environment due to the attractive electrostatic interactions between anions and positively charged surface. Thus, the effective concentration of phosphate anions inside the nanochannels is expected to be higher than the bulk concentration due to preconcentration effects. As the surface charge remains positive, this situation holds for the whole phosphate concentration range at pH 5, yielding a great increment of the apparent binding constant (in terms of the bulk concentrations).

In the case of pH 7 and 9, the contribution of the nanoconfinement effect is less straightforward. Although the previously described effects appear at low Pi concentrations (positive surface charge of the nanochannel), the opposite effect is expected for high Pi concentrations, as the negative surface charge of the nanopore tends to reduce the phosphate concentration within the nanochannel. Thus, the effective binding constants would reflect the compromise between these

DOI: 10.1021/acs.jpcc.9b07977
J. Phys. Chem. C 2019, 123, 28997−29007

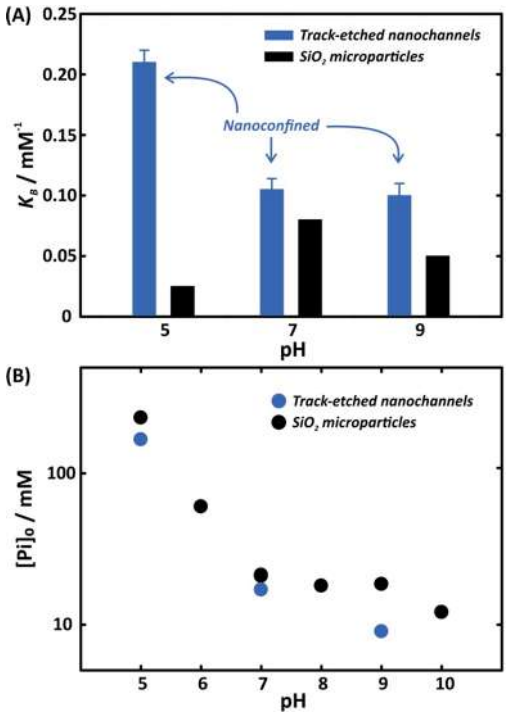

Figure 3. (A) Phosphate binding constant and (B) Pi concentration of zero net surface charge obtained from the study of modified nanochannels at different pH. Previously reported results for the binding to PAH-functionalized SiO_2 microparticles are added for comparison.[63]

opposite tendencies. Results in Figure 3A show that the higher nanoconfinement effect in the positive surface charge regime seems to dominate the binding behavior, yielding higher apparent binding constants in the case of nanochannels.

Confinement effects have been already shown to favor the uncharged states at the surface of nanochannels.[49] As an example, in the case of acid−base equilibrium, a shift in the chemical potential compared to the bulk value is observed, which reduces the proportion of charged species to minimize the electrostatic repulsion. Thus, reducing the nanochannel diameter leads to an increase in the acid dissociation pK_a[49] (charged species as a product of the chemical equilibrium), whereas it decreases the pK_a of base protonation (charged species as reagent of the chemical equilibrium).[50] We hypothesize that a similar effect is also occurring for the phosphate binding equilibrium within the nanochannels. Compared to the case of microparticles, phosphate bulk concentrations required to null the nanochannels surface charge is lower, independently of the pH of the solution (Figure 3B), meaning that the uncharged species are stabilized within the nanochannels compared to the surface of the microparticles.

It is interesting to note that our comparison of the binding equilibrium to study confinement effects does not take into account the effects stemming from the surface-confinement as both systems (microparticles and nanochannels) present the binding equilibrium to surface-confined amino groups. Therefore, differences observed in Figure 3 can be interpreted as coming from the confinement of the chemical equilibrium to the reduced environment of the nanochannels volume and the curvature of the surface (particularly, in the tip region).[49,50,71,72]

Direct comparison with bulk binding parameters is not straightforward in the present case, as the bulk behavior of the PAH-phosphate binding equilibrium presents additional

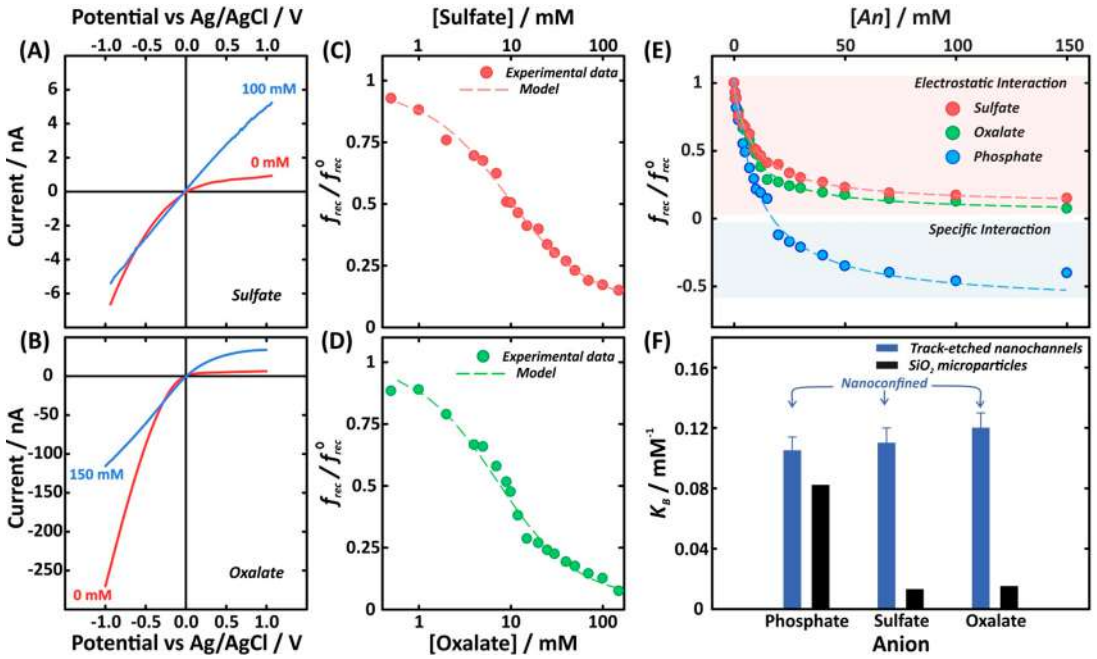

Figure 4. *I*−*V* curves in the absence (red) and presence of high concentration of divalent anions (blue): (A) sulfate and (B) oxalate. Relative rectification factor for increasing sulfate (C) and oxalate (D) concentrations in log scale. Dashed lines correspond to the fittings to experimental data with the binding model. (E) Relative rectification factor for increasing divalent anion concentrations. (F) Comparison between binding constant obtained in PAH-functionalized track-etched nanochannels (blue) and PAH-functionalized microparticles (black) for the different anions. All measurements were carried out in 0.1 M KCl pH 7.

DOI: 10.1021/acs.jpcc.9b07977
J. Phys. Chem. C 2019, 123, 28997−29007

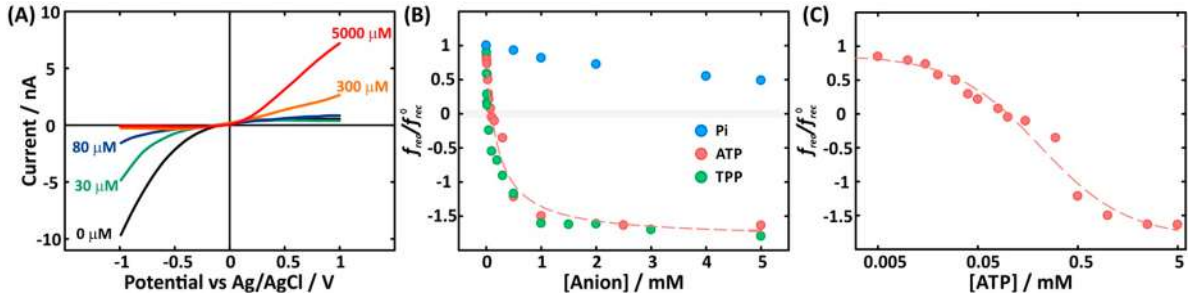

Figure 5. (A) $I-V$ curves of a PAH-modified single nanochannel at different concentrations of ATP. (B) Variation of relative rectification factor in the presence of simple phosphate (blue), ATP (red), and TPP (green). (C) Relative rectification factor for increasing ATP concentration. The x-log scale allows visualizing the good agreement between the experimental results and the binding model (dashed line). All measurements were carried out in 0.1 M KCl pH 7.

complexities coming from the formation of aggregates.[51,52,54,73] However, a relatively simple binding model has been recently developed to account for the phosphate concentration and pH effects in bulk.[51]

3.2. Specificity of Phosphate Binding. The selectivity of phosphate binding to amines was investigated by analyzing the dependence of the rectification factors on the concentration of other divalent anions at a constant pH value of 7. Sulfate and oxalate were employed for these assays as they are completely ionized (net charge: −2) in the pH range from 5 to 9. The experimental $I-V$ curves and the behavior of the relative rectification factors on the anion concentrations are shown in Figure 4. In Figure 4E, the values for phosphate were also added for comparison. Results in Figure 4A−D indicate that, as in the case of phosphate, certain binding of the divalent anions exists, leading to a decrease in the surface charge of the nanochannels that appears as changes in the $I-V$ curves and as a continuous diminution of the rectification factor. However, the limit behavior is quite different as there is no reversion of the surface charge in the case of sulfate and oxalate. However, they both present the same behavior. Thus, the results for sulfate and oxalate anions can be ascribed to their divalent valence, revealing that some specific effects are present in the case of phosphate, which can be ascribed as chemical effects as they depend on the chemical nature of the anion. The quantitative analysis of data for sulfate and oxalate in terms of the binding model yielded the parameters reported in Table 1. The good agreement of the fittings with the experimental results (dashed line in Figure 4B and D) reinforces the suitability of the binding model for describing the anion influence on the iontronic response of the amine-functionalized nanochannels.

Comparison with results on microparticles[63] again shows the confinement effects. The apparent binding constants for sulfate and oxalate are 1 order of magnitude higher in the case of nanochannels (Figure 4F). Having practically the same quantitative binding behavior, the results for sulfate and oxalate can be ascribed to the electrostatic interactions of divalent anions with the protonated surface amine groups. As no charge reversion is attained with sulfate and oxalate, the increment in the apparent binding constant can be rationalized in terms of the enhancement of the anion concentration within the positively charged nanochannels as explained above. In the case of phosphate, the charge reversion makes the analysis of the confinement effect on the binding constant more complex. Furthermore, the appearance of charge reversion only for the phosphate anion supports the idea that the chemical identity of binding anions becomes important when studying amine-functionalized surfaces compared to purely electrostatic phenomena.

As explained above, the confinement effects hinder the appearance of net charge on the nanochannel walls. The binding of phosphates continues even after the surface charge is neutralized. This fact reinforces the idea of specific interactions between this anion and the amino-functionalized surface. Even more, the binding takes place against the electrostatic interactions, evidencing the strength of these specific interactions. Charge reversion phenomena are usual when studying the adsorption of polyelectrolytes, proteins or other multiply charged species, where entropic effects are ascribed to be responsible for this apparently electrostatically forbidden situation. However, in the case of simple phosphate anions, this kind of entropic effect does not hold.

On the contrary, the specific interactions between phosphate and amine moieties have been ascribed to the possibility of hydrogen bonding.[74] The relevance of hydrogen-bond interactions has been recognized in the formation of supramolecular assemblies between polyamines and phosphates,[55] as a requisite for the stabilization of three-dimensional aggregates.[51,75]

Previous results suggest the idea that the interaction between amines and phosphates promotes both a higher protonation degree of the amines and a higher dissociation degree of the anions.[63] Kooijman and co-workers have also postulated the *electrostatic/hydrogen bond switch model* for the interaction of specific amine-rich protein domains and phosphate derivatives in biological membranes.[74,76] The present results indicate that a similar mechanism could operate in the interaction between amine surface groups and phosphate anions within the nanochannels, yielding high charge reversion values.

.

3.3. ATP Binding. Being a biorelevant phosphate species, the influence of the presence of adenosine triphosphate (ATP) on the iontronic output of PAH-modified nanochannels was also studied. Figure 5A shows the $I-V$ iontronic response of a PAH-modified single nanochannel after adding increasing concentrations of ATP in 0.1 M KCl at pH 7. At neutral pH, ATP is mainly in the tri- and tetravalent anion state. Again, the nanochannel initially presents a cation-driven diode-like behavior owing to the presence of positive surface charges. The ionic current then decreases when adding ATP to the electrolyte solution. This change is caused by the association of the multivalent anion to the amine surface groups as in the case

DOI: 10.1021/acs.jpcc.9b07977
J. Phys. Chem. C 2019, 123, 28997−29007

of phosphate. However, the changes appear in the submicromolar range for ATP. Thus, as it happens in the ATP-regulated K^+ channels (K_{ATP}),[8] the ionic flux through the nanochannel is highly sensitive to the presence of ATP, producing a diminution in the ionic flux that yields an OFF state for ATP concentrations of about 80 μM.[10,11] In the case of PAH-modified nanochannels, subsequent addition of higher concentrations of ATP ([ATP] > 80 μM) led to the appearance of a new non-Ohmic response, with a cation-driven diode-like behavior, revealing surface charge reversion. Thus, remarkably, the system can vary from anion selectivity to nonselectivity or cation selectivity with an ATP concentration of ~0.08−0.1 mM.

Figure 5B and C shows the relative rectification factor for various ATP concentrations. The dashed line corresponds to the values predicted by the model evidencing again a good correlation between experimental results and the binding model. By analyzing the iontronic response as a function of the ATP concentration in terms of the binding model, both the binding constant and the concentration for null surface charge, $[ATP]_0$, were determined (Table 1).

The binding model is based on the assumption that the change in the iontronic behavior is mainly determined by the surface charge density (see the Appendix). However, in the case of ATP, other effects such as hydrophobicity changes or reduction of the effective nanopore diameter[45] could operate.

In order to explore the relative importance of the electrostatic effects, the iontronic behavior in the presence of tripolyphosphate anion (TPP) was also studied. This anion constitutes the inorganic part of ATP, so that effects induced by the presence of the organic moiety (adenosine) could be discarded. Results included in Figure 5B indicate the same quantitative behavior for ATP and TPP, enhancing the importance of the electrostatic effects and supporting the application of the binding model also in the case of ATP.

As shown in Table 1, the iontronic response is much more sensitive to ATP compared to simple phosphate anions, as it could be expected from the higher negative charge. This idea was tested by studying the effect of ATP concentration on the zeta potential of PAH-modified silica microparticles (Supporting Information). As shown in Figure S4, the addition of ATP leads to a decrease of the zeta potential and subsequent reversion of the surface charge of the microparticles as in the case of Pi. However, in the case of ATP, changes in the rectification factor take place in a lower concentration range and a higher reversion percentage is attained for high concentrations.

In the case of the nanochannels, for ATP concentrations around 80 μM, the ionic binding produces neutralization of positive charges. When the ATP concentration exceeds 80 μM, the charge reversion produced by ionic binding leads to a prevalence of negative charges in the channel with the concomitant effect on the $I-V$ curve.

In a previous work with smaller nanochannels (tip diameter ≈ 6 nm) modified with polyethyleneimine (PEI), the presence of ATP was reported to produce a decrease in the ionic transmembrane current without evidence of surface charge reversion even at 1 mM concentration.[45] This apparent contradiction with our results comes from some important differences between both nanofluidic systems. First, PEI contains amino groups of different nature that can modify both the protonation behavior and the interaction with phosphates. Moreover, in the present work, the tip diameter is around ~40 nm,[22,44,77] and the steric hindrance by the ATP molecules in the nanochannel tip could be negligible.

Figure 5B shows the changes in the relative rectification factor with increasing ATP and Pi concentration. As described above, the increment of both ATP and Pi produced a diminution in the relative rectification factor owing to the phosphate binding to the amine group. However, the iontronic response is much more sensitive to ATP.

Taking into account the higher sensibility of this system toward ATP, the sensing behavior at low ATP concentrations was explored (Figure 6). The system exhibited not only a great sensibility but also a good linear relation for low concentrations of ATP. These results are promising facing the design of simple and very sensitive nanopore detection platforms exploiting biomimetic interactions.

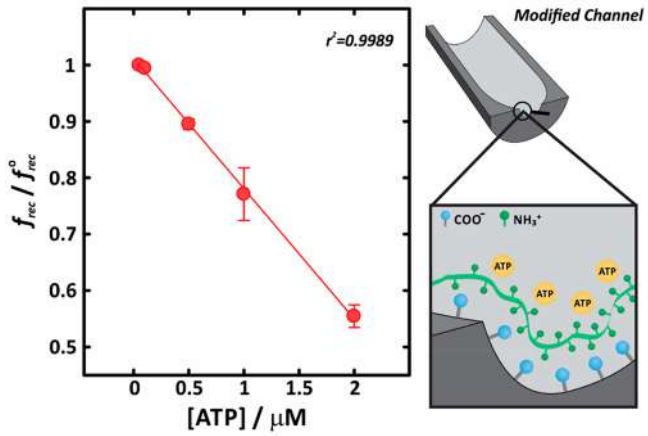

Figure 6. Change of the relative rectification factor at low ATP concentrations and scheme of the sensing mechanism. The system shows excellent linearity for biorelevant concentrations of ATP.

4. CONCLUSIONS

In summary, we have carried out an extensive study of the amine-phosphate interactions within solid-state nanochannels by measuring the changes in the iontronic transmembrane current response on PAH-functionalized single pore channels in the presence of different anions at different pH values. By a simple ion binding scheme, it is possible to model the binding of charged amines and phosphate anions to account for the differences in the charge state of surface groups, detectable as changes in the asymmetry of the diode-like iontronic transmembrane response. The binding model is shown to satisfactorily describe the iontronic response in terms of the rectification factors for the studied systems.

Particularly in the case of phosphate, the binding takes place even in electrostatically hindered conditions as revealed by the iontronic results, which reinforces the idea of chemical specificity of the amine−phosphate interaction. The origin of this specificity is probably caused by the possibility of hydrogen bonding formation.

Furthermore, the effects of nanoconfinement on this equilibrium were analyzed by comparison with previous results on the phosphate−amine binding equilibrium on PAH-modified SiO_2 microparticles. Owing to the confinement to the small environment of the nanochannel interior, the binding constants are 1 order of magnitude higher for the binding of divalent anions to the positively charged nanochannels. Charge

DOI: 10.1021/acs.jpcc.9b07977
J. Phys. Chem. C 2019, 123, 28997−29007

reversion takes place even at lower phosphate concentrations. In contrast, polyphosphates showed a more pronounced binding behavior toward amine moieties, which allowed the detection and quantification of ATP in the micromolar range.

The present results and analysis open the door to study other relevant chemical equilibrium situations within nanochannels. We expect that they will stimulate the use of nanofluidic devices as source of physicochemical answers to questions arising from nanoconfinement phenomena.

APPENDIX

Binding Model for the Iontronic Response

For a quantitative analysis of the iontronic responses as a function of the anion concentration, we developed a simple binding model as follows.[63]

As the pH range considered is 5−9, the only relevant phosphate species will be the mono and divalent anions, according to this equilibrium

$$H_2PO_4^- \leftrightarrow HPO_4^{-2} + H^+ \quad pK_{a2} = 7.2$$

In the case of sulfate and oxalate, the measurements were performed at pH 7, so just the divalent forms of these anions were considered. Moreover, the interaction between chloride and amine groups was neglected as it is well-known to be weak.[43,78]

Additionally, we also take into account the presence of negative surface charges in the unmodified PET track-etched nanochannels.[68]

Thus, the following equilibriums are considered,

$$(R{-}NH_3^+) + H_2PO_4^- \leftrightarrow (R{-}NH_5PO_4) \quad K_{11}$$

$$(R{-}NH_3^+) + HPO_4^{2-} \leftrightarrow (R{-}NH_4PO_4)^- \quad K_{12}$$

$$(R{-}NH_3^+) \leftrightarrow (R{-}NH_2) + H^+ \quad K_a$$

where brackets are employed for surface-confined species.

The binding of charged species to the nanochannel wall induces changes in the surface charge density (σ). This charge density is proportional to the surface concentration of the different charged groups:

$$\sigma \propto [(R{-}NH_3^+)] - [(R{-}NH_4PO_4^-)] - [(-COO^-)] \tag{A.1}$$

where $-COO^-$ means the carboxylate groups from the etched PET. By defining the dissociation degree of the bound phosphate species as

$$\alpha_- = \frac{[(R{-}NH_4PO_4^-)]}{[(R{-}NH_4PO_4^-)] + [(R{-}NH_5PO_4)]} \tag{A.2}$$

Related to the dissociation equilibrium of surface confided phosphate species

$$(R{-}NH_5PO_4) \leftrightarrow (R{-}NH_4PO_4)^- + H^+ \quad K_{a2,app} = K_{a2}\frac{K_{12}}{K_{11}}$$

Using this expression, eq A.1 can be rewritten as

$$\sigma \propto [(R{-}NH_3^+)]\{1 - K_B\alpha_-[Pi]\} - [(-COO^-)] \tag{A.3}$$

where [Pi] means the total phosphate bulk concentration (or analytical concentration), which in this pH range can be written as $[Pi] = [H_2PO_4^-] + [HPO_4^{2-}]$, and K_B means the global phosphate binding constant,

$$K_B = \alpha_1 K_{11} + \alpha_2 K_{12} \tag{A.4}$$

where α_1 and α_2 mean the distribution functions for the monovalent and divalent phosphate species in solution, respectively.

On the other hand, by considering the total concentration of amine surface groups,

$$\Gamma_{NH_2} = [(R{-}NH_2)] + [(R{-}NH_3^+)] + [(R{-}NH_4PO_4^-)] + [(R{-}NH_5PO_4)] \tag{A.5}$$

which can be rewritten as

$$\Gamma_{NH_2} = [(R{-}NH_3^+)]\left\{1 + \frac{[(R{-}NH_2)]}{[(R{-}NH_3^+)]} + K_B[Pi]\right\} \tag{A.6}$$

Using this last expression, eq A.3 becomes

$$\sigma \propto \frac{\Gamma_{NH_2}\{1 - K_B\alpha_-[Pi]\}}{\left\{1 + \frac{[(R{-}NH_2)]}{[(R{-}NH_3^+)]} + K_B[Pi]\right\}} - [(R{-}COO^-)] \tag{A.7}$$

In the absence of anion binding,

$$\sigma_0 \propto \frac{\Gamma_{NH_2}}{\left\{1 + \frac{[(R{-}NH_2)]}{[(R{-}NH_3^+)]}\right\}} - [(R{-}COO^-)] \tag{A.8}$$

whereas for phosphate binding saturation,

$$\sigma_\infty \propto -\Gamma_{NH_2}\alpha_- - [(R{-}COO^-)] \tag{A.9}$$

Using these last expressions, it is possible to find the following relation between the surface charge density and the anion concentration

$$\frac{\sigma_0 - \sigma}{\sigma_0 - \sigma_\infty} = \frac{K_B\theta_+[Pi]}{1 + K_B\theta_+[Pi]} \tag{A.10}$$

where

$$\theta_+ = \frac{[(R{-}NH_3^+)]}{[(R{-}NH_3^+)] + [(R{-}NH_2)]} \tag{A.11}$$

Rearranging eq. A.10, it results into

$$\frac{\sigma}{\sigma_0} = \frac{1 - C[Pi]}{1 + B[Pi]} \tag{A.12}$$

where B and C are constants for a given pH value.

Changes in the surface charge density can be correlated to changes in the rectification factors. Particularly, it has been proved that, for low surface charge, there is a linear relationship between σ and f_{rec},[68] which allows writing

$$\frac{f_{rec}}{f_{rec}^0} = \frac{1 - C[Pi]}{1 + B[Pi]} \tag{A.13}$$

with f_{rec}^0 being the value in the absence of binding anions and

$$C = \left(-\frac{f_{rec}^\infty}{f_{rec}^0}\right)K_B\theta_+ \tag{A.14}$$

$$B = K_B\theta_+ \tag{A.15}$$

DOI: 10.1021/acs.jpcc.9b07977
J. Phys. Chem. C 2019, 123, 28997−29007

where f_{rec}^{∞} is the rectification factor for high binding anion concentrations. From constant B and the reported values for θ_+,[68] the binding constants were obtained by nonlinear fitting.

In the case of divalent anions, such as sulfate and oxalate, whose pK_{a2} values are low enough to neglect the contribution of monovalent species, eq A.13 is also valid. Then, the general expression can be written as

$$\frac{f_{rec}}{f_{rec}^{0}} = \frac{1 - C[An]}{1 + B[An]} \tag{A.16}$$

where [An] corresponds to the analytical concentration of the anion. From eq A.16, it is possible to define the anion concentration for inducing zero net surface charge,

$$[An]_0 = \frac{1}{C} \tag{A.17}$$

and the charge reversion degree, $R(\%)$, as

$$R(\%) = -100\frac{f_{rec}^{\infty}}{f_{rec}^{0}} = 100\frac{C}{B} \tag{A.18}$$

It is important to clarify that, within the model, changes in the rectification factor owing to variations in the ionic strength or diminution of the effective diameter were not taken into account. However, as demonstrated by experimental results in Figures 5 and S1, these effects are negligible compared to the changes triggered for the ionic pair formation.

■ ASSOCIATED CONTENT

Supporting Information

The Supporting Information is available free of charge on the ACS Publications website at DOI: 10.1021/acs.jpcc.9b07977.

Additional results on the iontronic response of unmodified nanochannels, PAH-functionalized nanochannels at different pH values, and zeta potential of PAH-functionalized silica microparticles in the presence of ATP (PDF)

■ AUTHOR INFORMATION

Corresponding Authors

*E-mail: wmarmi@inifta.unlp.edu.ar (W.A.M.). Web: http://softmatter.quimica.unlp.edu.ar. Twitter: @softmatterlab.

*E-mail: azzaroni@inifta.unlp.edu.ar (O.A.).

ORCID

Waldemar A. Marmisollé: 0000-0003-0031-5371

Omar Azzaroni: 0000-0002-5098-0612

Present Address

‖G.P.-M.: Laboratory of Molecular Neurobiology and Biophysics, Howard Hughes Medical Institute, The Rockefeller University, 1230 York Avenue, New York, New York 10065, United States.

Author Contributions

The manuscript was written through contributions of all authors. All authors have given approval to the final version of the manuscript.

Notes

The authors declare no competing financial interest.

■ ACKNOWLEDGMENTS

G.L. and G.P.-M. acknowledge a doctoral scholarship from CONICET. W.A.M. and O.A. are CONICET fellows and acknowledge financial support from Universidad Nacional de La Plata (PPID-X016), CONICET (PIP-0370), and ANPCyT (PICT-2017-1523 and PICT2016-1680). Financial support provided by the German Academic Exchange Service (DAAD) is acknowledged by G.P.-M. C.T. and M.E.T.-M. thank the LOEWE project iNAPO funded by the Ministry of Higher Education, Research and the Arts (HMWK) of the Hessen state. The results presented here are based on a UMAT experiment, which was performed at the X0-beamline of the UNILAC at the GSI Helmholtzzentrum für Schwerionenforschung, Darmstadt (Germany) in the frame of FAIR Phase-0.

■ REFERENCES

(1) Vincent, J. F. V. Biomimetics - A Review. *Proc. Inst. Mech. Eng., Part H* **2009**, *223* (8), 919−939.

(2) Li, J.; He, Q.; Yan, X. *Molecular Assembly of Biomimetic Systems*; VCH-Wiley; Weinheim, 2011.

(3) Jiang, L.; Feng, L. *Bioinspired Intelligent Nanostructured Interfacial Materials*; World Scientific Publishing Company: Singapore, 2010; Vol. 38.

(4) Kumar, C. S. S. R. *Biomimetic and Bioinspired Nanomaterials*; Weinheim: VCH-Wiley, 2010.

(5) Pérez-Mitta, G.; Albesa, A. G.; Trautmann, C.; Toimil-Molares, M. E.; Azzaroni, O. Bioinspired Integrated Nanosystems Based on Solid-State Nanopores: "Iontronic" Transduction of Biological, Chemical and Physical Stimuli. *Chem. Sci.* **2017**, *8* (2), 890−913.

(6) Zhang, Z.; Wen, L.; Jiang, L. Bioinspired Smart Asymmetric Nanochannel Membranes. *Chem. Soc. Rev.* **2018**, *47* (2), 322−356.

(7) Dekker, C. Solid-State Nanopores. *Nat. Nanotechnol.* **2007**, *2* (4), 209−215.

(8) Hille, B. *Ion Channels of Excitable Membranes*, 3rd ed.; Sinauer Associates: Sunderland, MA, 2001.

(9) Aguilar-Bryan, L.; Bryan, J. Molecular Biology of Adenosine Triphosphate-Sensitive Potassium Channels. *Endocr. Rev.* **1999**, *20* (2), 101−135.

(10) Noma, A. ATP-Regulated K+ Channels in Cardiac Muscle. *Nature* **1983**, *305* (5930), 147−148.

(11) Takano, M.; Noma, A. The ATP-Sensitive K+ Channel. *Prog. Neurobiol.* **1993**, *41* (1), 21−30.

(12) Cook, D. L.; Hales, N. Intracellular ATP Directly Blocks K+ Channels in Pancreatic B-Cells. *Nature* **1984**, *311* (5983), 271−273.

(13) Siwy, Z. S. Ion-Current Rectification in Nanopores and Nanotubes with Broken Symmetry. *Adv. Funct. Mater.* **2006**, *16* (6), 735−746.

(14) Siwy, Z.; Fuliński, A. Fabrication of a Synthetic Nanopore Ion Pump. *Phys. Rev. Lett.* **2002**, *89* (19), 4−7.

(15) Vilozny, B.; Wollenberg, A. L.; Actis, P.; Hwang, D.; Singaram, B.; Pourmand, N. Carbohydrate-Actuated Nanofluidic Diode: Switchable Current Rectification in a Nanopipette. *Nanoscale* **2013**, *5* (19), 9214.

(16) Wang, M.; Meng, H.; Wang, D.; Yin, Y.; Stroeve, P.; Zhang, Y.; Sheng, Z.; Chen, B.; Zhan, K.; Hou, X. Dynamic Curvature Nanochannel-Based Membrane with Anomalous Ionic Transport Behaviors and Reversible Rectification Switch. *Adv. Mater.* **2019**, *31* (11), 1805130.

(17) Vlassiouk, I.; Siwy, Z. S. Nanofluidic Diode. *Nano Lett.* **2007**, *7* (3), 552−556.

(18) Zhang, H.; Hou, X.; Hou, J.; Zeng, L.; Tian, Y.; Li, L.; Jiang, L. Synthetic Asymmetric-Shaped Nanodevices with Symmetric PH-Gating Characteristics. *Adv. Funct. Mater.* **2015**, *25* (7), 1102−1110.

(19) Wong, H.-S.; Akinwande, D. *Carbon Nanotube and Graphene Device Physics*; Cambridge University Press, 2011.

(20) Ramírez, P.; Apel, P. Y.; Cervera, J.; Mafé, S. Pore Structure and Function of Synthetic Nanopores with Fixed Charges: Tip Shape and Rectification Properties. *Nanotechnology* **2008**, *19* (31), 315707.

(21) Hou, X.; Zhang, H.; Jiang, L. Building Bio-Inspired Artificial Functional Nanochannels: From Symmetric to Asymmetric Modification. *Angew. Chem., Int. Ed.* **2012**, *51* (22), 5296−5307.

(22) Pérez-Mitta, G.; Albesa, A. G.; Knoll, W.; Trautmann, C.; Toimil-Molares, M. E.; Azzaroni, O. Host-Guest Supramolecular Chemistry in Solid-State Nanopores: Potassium-Driven Modulation of Ionic Transport in Nanofluidic Diodes. *Nanoscale* **2015**, *7* (38), 15594−15598.
(23) Yameen, B.; Ali, M.; Neumann, R.; Ensinger, W.; Knoll, W.; Azzaroni, O. Synthetic Proton-Gated Ion Channels via Single Solid-State Nanochannels Modified with Responsive Polymer Brushes. *Nano Lett.* **2009**, *9* (7), 2788−2793.
(24) Ali, M.; Yameen, B.; Neumann, R.; Ensinger, W.; Knoll, W.; Azzaroni, O. Biosensing and Supramolecular Bioconjugation in Single Conical Polymer Nanochannels. Facile Incorporation of Biorecognition Elements into Nanoconfined Geometries. *J. Am. Chem. Soc.* **2008**, *130*, 16351−16357.
(25) Actis, P.; Jejelowo, O.; Pourmand, N. Ultrasensitive Mycotoxin Detection by STING Sensors. *Biosens. Bioelectron.* **2010**, *26* (2), 333−337.
(26) Actis, P.; Mak, A. C.; Pourmand, N. Functionalized Nanopipettes: Toward Label-Free, Single Cell Biosensors. *Bioanal. Rev.* **2010**, *1* (2−4), 177−185.
(27) Mayne, L.; Lin, C.-Y.; Christie, S. D. R.; Siwy, Z. S.; Platt, M. The Design and Characterization of Multifunctional Aptamer Nanopore Sensors. *ACS Nano* **2018**, *12* (5), 4844−4852.
(28) Xin, W.; Zhang, Z.; Huang, X.; Hu, Y.; Zhou, T.; Zhu, C.; Kong, X.-Y.; Jiang, L.; Wen, L. High-Performance Silk-Based Hybrid Membranes Employed for Osmotic Energy Conversion. *Nat. Commun.* **2019**, *10* (1), 3876.
(29) Zhu, Y.; Zhan, K.; Hou, X. Interface Design of Nanochannels for Energy Utilization. *ACS Nano* **2018**, *12* (2), 908−911.
(30) Pérez-Mitta, G.; Marmisollé, W. A.; Trautmann, C.; Toimil-Molares, M. E.; Azzaroni, O. An All-Plastic Field-Effect Nanofluidic Diode Gated by a Conducting Polymer Layer. *Adv. Mater.* **2017**, *29*, 1700972.
(31) Huang, X.; Kong, X.; Wen, L.; Jiang, L. Bioinspired Ionic Diodes: From Unipolar to Bipolar. *Adv. Funct. Mater.* **2018**, *28* (49), 1801079.
(32) Zhu, Z.; Wang, D.; Tian, Y.; Jiang, L. Ion/Molecule Transportation in Nanopores and Nanochannels: From Critical Principles to Diverse Functions. *J. Am. Chem. Soc.* **2019**, *141* (22), 8658−8669.
(33) Guan, W.; Fan, R.; Reed, M. A. Field-Effect Reconfigurable Nanofluidic Ionic Diodes. *Nat. Commun.* **2011**, *2* (1), 506.
(34) Tian, Y.; Wen, L.; Hou, X.; Hou, G.; Jiang, L. Bioinspired Ion-Transport Properties of Solid-State Single Nanochannels and Their Applications in Sensing. *ChemPhysChem* **2012**, *13* (10), 2455−2470.
(35) Li, P.; Xie, G.; Kong, X. Y.; Zhang, Z.; Xiao, K.; Wen, L.; Jiang, L. Light-Controlled Ion Transport through Biomimetic DNA-Based Channels. *Angew. Chem., Int. Ed.* **2016**, *55* (50), 15637−15641.
(36) Hou, G.; Wang, D.; Xiao, K.; Zhang, H.; Zheng, S.; Li, P.; Tian, Y.; Jiang, L. Magnetic Gated Biomimetic Artificial Nanochannels for Controllable Ion Transportation Inspired by Homing Pigeon. *Small* **2018**, *14* (18), 1703369.
(37) Siwy, Z. S.; Powell, M. R.; Petrov, A.; Kalman, E.; Trautmann, C.; Eisenberg, R. S. Calcium-Induced Voltage Gating in Single Conical Nanopores. *Nano Lett.* **2006**, *6* (8), 1729−1734.
(38) Pérez-Mitta, G.; Marmisolle, W. A.; Burr, L.; Toimil-Molares, M. E.; Trautmann, C.; Azzaroni, O. Proton-Gated Rectification Regimes in Nanofluidic Diodes Switched by Chemical Effectors. *Small* **2018**, *14*, 1703144.
(39) Pérez-Mitta, G.; Toimil-Molares, M. E.; Trautmann, C.; Marmisollé, W. A.; Azzaroni, O. Molecular Design of Solid-State Nanopores: Fundamental Concepts and Applications. *Adv. Mater.* **2019**, *31*, 1901483.
(40) Xiao, K.; Wen, L.; Jiang, L. Biomimetic Solid-State Nanochannels: From Fundamental Research to Practical Applications. *Small* **2016**, *12* (21), 2810−2831.
(41) Xie, G.; Li, P.; Zhao, Z.; Zhu, Z.; Kong, X.-Y. Y.; Zhang, Z.; Xiao, K.; Wen, L.; Jiang, L. Light- and Electric-Field-Controlled Wetting Behavior in Nanochannels for Regulating Nanoconfined Mass Transport. *J. Am. Chem. Soc.* **2018**, *140* (13), 4552−4559.
(42) Ali, M.; Tahir, M. N.; Siwy, Z.; Neumann, R.; Tremel, W.; Ensinger, W. Hydrogen Peroxide Sensing with Horseradish Peroxidase-Modified Polymer Single Conical Nanochannels. *Anal. Chem.* **2011**, *83* (5), 1673−1680.
(43) Pérez-Mitta, G.; Marmisollé, W. A.; Albesa, A. G.; Toimil-Molares, M. E.; Trautmann, C.; Azzaroni, O. Phosphate-Responsive Biomimetic Nanofluidic Diodes Regulated by Polyamine-Phosphate Interactions: Insights into Their Functional Behavior from Theory and Experiment. *Small* **2018**, *14* (18), 1702131.
(44) Pérez-Mitta, G.; Peinetti, A. S.; Cortez, M. L.; Toimil-Molares, M. E.; Trautmann, C.; Azzaroni, O. Highly Sensitive Biosensing with Solid-State Nanopores Displaying Enzymatically Reconfigurable Rectification Properties. *Nano Lett.* **2018**, *18* (5), 3303−3310.
(45) Ali, M.; Nguyen, Q. H.; Neumann, R.; Ensinger, W. ATP-Modulated Ionic Transport through Synthetic Nanochannels. *Chem. Commun.* **2010**, *46* (36), 6690.
(46) Gao, L.; Li, P.; Zhang, Y.; Xiao, K.; Ma, J.; Xie, G.; Hou, G.; Zhang, Z.; Wen, L.; Jiang, L. A Bio-Inspired, Sensitive, and Selective Ionic Gate Driven by Silver (I) Ions. *Small* **2015**, *11* (5), 543−547.
(47) Shi, W.; Friedman, A. K.; Baker, L. A. Nanopore Sensing. *Anal. Chem.* **2017**, *89* (1), 157−188.
(48) Haywood, D. G.; Saha-Shah, A.; Baker, L. A.; Jacobson, S. C. Fundamental Studies of Nanofluidics: Nanopores, Nanochannels, and Nanopipets. *Anal. Chem.* **2015**, *87* (1), 172−187.
(49) Gilles, F. M.; Tagliazucchi, M.; Azzaroni, O.; Szleifer, I. Ionic Conductance of Polyelectrolyte-Modified Nanochannels: Nanoconfinement Effects on the Coupled Protonation Equilibria of Polyprotic Brushes. *J. Phys. Chem. C* **2016**, *120* (9), 4789−4798.
(50) Tagliazucchi, M.; Azzaroni, O.; Szleifer, I. Responsive Polymers End-Tethered in Solid-State Nanochannels: When Nanoconfinement Really Matters. *J. Am. Chem. Soc.* **2010**, *132* (35), 12404−12411.
(51) Herrera, S. E.; Agazzi, M. L.; Cortez, M. L.; Marmisollé, W. A.; Tagliazucchi, M.; Azzaroni, O. Polyamine Colloids Cross-Linked with Phosphate Ions: Towards Understanding the Solution Phase Behavior. *ChemPhysChem* **2019**, *20* (8), 1044−1053.
(52) Agazzi, M. L.; Herrera, S. E.; Cortez, M. L.; Marmisollé, W. A.; Von Bilderling, C.; Pietrasanta, L. I.; Azzaroni, O. Continuous Assembly of Supramolecular Polyamine-Phosphate Networks on Surfaces: Preparation and Permeability Properties of Nanofilms. *Soft Matter* **2019**, *15* (7), 1640−1650.
(53) Andreozzi, P.; Diamanti, E.; Py-Daniel, K. R.; Cáceres-Vélez, P. R.; Martinelli, C.; Politakos, N.; Escobar, A.; Muzi-Falconi, M.; Azevedo, R.; Moya, S. E. Exploring the PH Sensitivity of Poly(Allylamine) Phosphate Supramolecular Nanocarriers for Intracellular SiRNA Delivery. *ACS Appl. Mater. Interfaces* **2017**, *9* (44), 38242−38254.
(54) Muzzio, N. E.; Pasquale, M. A.; Marmisollé, W. A.; Von Bilderling, C.; Cortez, M. L.; Pietrasanta, L. I.; Azzaroni, O. Self-Assembled Phosphate-Polyamine Networks as Biocompatible Supramolecular Platforms to Modulate Cell Adhesion. *Biomater. Sci.* **2018**, *6* (8), 2230−2247.
(55) Marmisollé, W. A.; Irigoyen, J.; Gregurec, D.; Moya, S.; Azzaroni, O. Supramolecular Surface Chemistry: Substrate-Independent, Phosphate-Driven Growth of Polyamine-Based Multifunctional Thin Films. *Adv. Funct. Mater.* **2015**, *25* (26), 4144−4152.
(56) Cortez, M. L.; Lorenzo, A.; Marmisollé, W. A.; von Bilderling, C.; Maza, E.; Pietrasanta, L.; Battaglini, F.; Ceolín, M.; Azzaroni, O. Highly-Organized Stacked Multilayers via Layer-by-Layer Assembly of Lipid-like Surfactants and Polyelectrolytes. Stratified Supramolecular Structures for (Bio)Electrochemical Nanoarchitectonics. *Soft Matter* **2018**, *14* (10), 1939−1952.
(57) Lorenzo, A.; Marmisollé, W. A.; Maza, E. M.; Ceolín, M.; Azzaroni, O. Electrochemical Nanoarchitectonics through Polyaminobenzylamine−Dodecyl Phosphate Complexes: Redox Activity and Mesoscopic Organization in Self-Assembled Nanofilms. *Phys. Chem. Chem. Phys.* **2018**, *20* (11), 7570−7578.

DOI: 10.1021/acs.jpcc.9b07977
J. Phys. Chem. C 2019, 123, 28997−29007

(58) D'Agostino, L.; Di Luccia, A. Polyamines Interact with DNA as Molecular Aggregates. *Eur. J. Biochem.* **2002**, *269* (17), 4317−4325.
(59) Di Luccia, A.; Picariello, G.; Iacomino, G.; Formisano, A.; Paduano, L.; D'Agostino, L. The in Vitro Nuclear Aggregates of Polyamines. *FEBS J.* **2009**, *276* (8), 2324−2335.
(60) Irigoyen, J.; Moya, S. E.; Iturri, J. J.; Llarena, I.; Azzaroni, O.; Donath, E. Specific ζ-Potential Response of Layer-by-Layer Coated Colloidal Particles Triggered by Polyelectrolyte Ion Interactions. *Langmuir* **2009**, *25* (6), 3374−3380.
(61) Capdevila, D. A.; Marmisollé, W. A.; Williams, F. J.; Murgida, D. H. Phosphate Mediated Adsorption and Electron Transfer of Cytochrome c. A Time-Resolved SERR Spectroelectrochemical Study. *Phys. Chem. Chem. Phys.* **2013**, *15* (15), 5386−5394.
(62) Marmisolle, W. A.; Capdevila, D. A.; de la Llave, E.; Williams, F. J.; Murgida, D. H. Self-Assembled Monolayers of NH2-Terminated Thiolates: Order, PKa, and Specific Adsorption. *Langmuir* **2013**, *29*, 5351−5359.
(63) Laucirica, G.; Marmisollé, W. A.; Azzaroni, O. Dangerous Liaisons: Anion-Induced Protonation in Phosphate-Polyamine Interactions and Their Implications for Charge States of Biologically Relevant Surfaces. *Phys. Chem. Chem. Phys.* **2017**, *19*, 8612−8620.
(64) Capdevila, D. A.; Marmisolle, W. A.; Tomasina, F.; Demicheli, V.; Portela, M.; Radi, R.; Murgida, D. H. Specific Methionine Oxidation of Cytochrome c in Complexes with Zwitterionic Lipids by Hydrogen Peroxide: Potential Implications for Apoptosis. *Chem. Sci.* **2015**, *6* (1), 705−713.
(65) Sumper, M. Biomimetic Patterning of Silica by Long-Chain Polyamines. *Angew. Chem., Int. Ed.* **2004**, *43* (17), 2251−2254.
(66) Brunner, E.; Lutz, K.; Sumper, M. Biomimetic Synthesis of Silica Nanospheres Depends on the Aggregation and Phase Separation of Polyamines in Aqueous Solution. *Phys. Chem. Chem. Phys.* **2004**, *6* (4), 854−857.
(67) Pérez-Mitta, G.; Marmisollé, W. A.; Albesa, A. G.; Toimil-Molares, M. E.; Trautmann, C.; Azzaroni, O. Phosphate-Responsive Biomimetic Nanofluidic Diodes Regulated by Polyamine-Phosphate Interactions: Insights into Their Functional Behavior from Theory and Experiment. *Small* **2018**, *14* (18), 1702131.
(68) Pérez-Mitta, G.; Albesa, A.; Gilles, F. M.; Toimil-Molares, M. E.; Trautmann, C.; Azzaroni, O. Noncovalent Approach toward the Construction of Nanofluidic Diodes with PH-Reversible Rectifying Properties: Insights from Theory and Experiment. *J. Phys. Chem. C* **2017**, *121* (16), 9070−9076.
(69) Apel, P. Y.; Blonskaya, I. V.; Orelovitch, O. L.; Ramirez, P.; Sartowska, B. A. Effect of Nanopore Geometry on Ion Current Rectification. *Nanotechnology* **2011**, *22* (17), 175302 DOI: 10.1088/0957-4484/22/17/175302.
(70) Cervera, J.; Schiedt, B.; Neumann, R.; Mafá, S.; Ramírez, P. Ionic Conduction, Rectification, and Selectivity in Single Conical Nanopores. *J. Chem. Phys.* **2006**, *124* (10), 104706.
(71) Nap, R.; Gong, P.; Szleifer, I. Weak Polyelectrolytes Tethered to Surfaces: Effect of Geometry, Acid−Base Equilibrium and Electrical Permittivity. *J. Polym. Sci., Part B: Polym. Phys.* **2006**, *44* (18), 2638−2662.
(72) Wang, D.; Nap, R. J.; Lagzi, I.; Kowalczyk, B.; Han, S.; Grzybowski, B. A.; Szleifer, I. How and Why Nanoparticle's Curvature Regulates the Apparent PKa of the Coating Ligands. *J. Am. Chem. Soc.* **2011**, *133* (7), 2192−2197.
(73) Marmisollé, W. A.; Gregurec, D.; Moya, S.; Azzaroni, O. Polyanilines with Pendant Amino Groups as Electrochemically Active Copolymers at Neutral PH. *ChemElectroChem* **2015**, *2* (12), 2011−2019.
(74) Kooijman, E. E.; Tieleman, D. P.; Testerink, C.; Munnik, T.; Rijkers, D. T. S.; Burger, K. N. J.; De Kruijff, B. An Electrostatic/Hydrogen Bond Switch as the Basis for the Specific Interaction of Phosphatidic Acid with Proteins. *J. Biol. Chem.* **2007**, *282* (15), 11356−11364.
(75) Lutz, K.; Gröger, C.; Sumper, M.; Brunner, E. Biomimetic Silica Formation: Analysis of the Phosphate-Induced Self-Assembly of Polyamines. *Phys. Chem. Chem. Phys.* **2005**, *7* (14), 2812−2815.
(76) Shin, J. J.; Loewen, C. J. Putting the PH into Phosphatidic Acid Signaling. *BMC Biol.* **2011**, *9*, 85.
(77) Pérez-Mitta, G.; Tuninetti, J. S.; Knoll, W.; Trautmann, C.; Toimil-Molares, M. E.; Azzaroni, O. Polydopamine Meets Solid-State Nanopores: A Bioinspired Integrative Surface Chemistry Approach To Tailor the Functional Properties of Nanofluidic Diodes. *J. Am. Chem. Soc.* **2015**, *137* (18), 6011−6017.
(78) Casasús, R.; Climent, E.; Marcos, M. D.; Martínez-Máñez, R.; Sancenón, F.; Soto, J.; Amorós, P.; Cano, J.; Ruiz, E. Dual Aperture Control on PH- and Anion-Driven Supramolecular Nanoscopic Hybrid Gate-like Ensembles. *J. Am. Chem. Soc.* **2008**, *130* (6), 1903−1917.

DOI: 10.1021/acs.jpcc.9b07977
J. Phys. Chem. C 2019, 123, 28997−29007